Journal of Materials Chemistry A

Accepted Manuscript

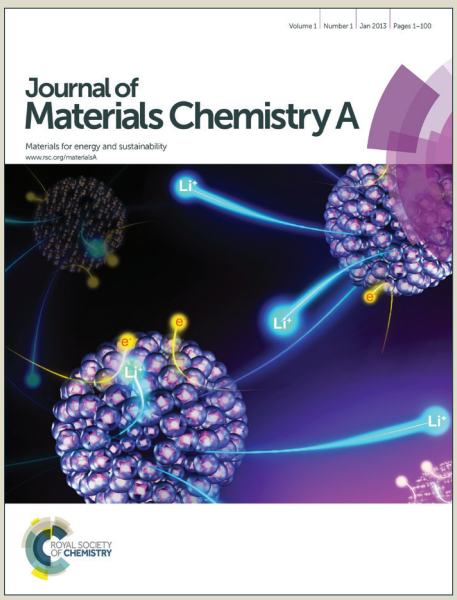

ROYAL SOCIETY OF CHEMISTRY

www.rsc.org/materialsA

Journal of Materials Chemistry A RSCPublishing

ARTICLE

InP and Sn:InP based quantum dot sensitized solar cells

Cite this: DOI: 10.1039/xoxxoooooox

Suolong Yang [a,b], Pengxiang Zhao[b] , Xiaochong Zhao[b] , Liangti Qu[a], Xinchun Lai[*b]

[a] Department of Chemistry, Beijing Institute of Technology, Beijing 100081, China.
[b] Science and Technology on Surface Physics and Chemistry Laboratory, Mianyang 621907, China.

Received ooth January 2012,
Accepted ooth January 2012

DOI: 10.1039/xoxxoooooox

www.rsc.org/

Due to the ideal band gap and environmental friendliness, InP is a promising light-harvesting material in photovoltaic cells. However, "green" InP based quantum dot sensitized solar cells (QDSSCs) have been rarely reported. Herein, nearly monodispersed Sn doped InP (Sn:InP) quantum dots (QDs) were synthesized by one-pot nucleation doping method, and used as the sensitizer in the construction of QDSSCs. High QDs loadings on the TiO_2 film electrodes were achieved *via* the capping ligand-induced self-assembly (CLIS) sensitization technique. The resulting champion Sn:InP cell shows a power conversion efficiency (PCE) of 3.54% under AM 1.5G (simulated 1 sun illumination), which is remarkably higher than that of un-doped InP QD based ones. This improvement is ascribed to the regulation role of the band gap by Sn dopant in the InP QDs. The Sn:InP QDSSCs exhibit moderate efficiency, good reproducibility and stability. These new findings may pave a way for the performance improvements of other QDs photovoltaic devices.

1. Introduction

Quantum dot sensitized solar cells (QDSSCs) have become one of the candidates for next generation solar cells, because of their unique properties, such as tunable light-harvesting range, low-cost and multiple-exciton effects, *etc.*[1-6] So far, many QDs materials have been used as the sensitizers for QDSSCs including CdS,[7] PbS,[8] CdSe[9-16] and $CuInS_2$.[17-22] Among all the QDSSCs, CdSe,[23] $CuInS_2$[24] and CdSe/CdTe[25] core/shell QDSSCs have shown high power conversion efficiency (PEC) of 5.4%, 7.04% and 8.21%, respectively. Although there are a lot of reports on the applications of QDs in QDSSCs, it is still highly desirable to explore new "green" Cd-free QDs materials such as InP QDs. InP QDs are considered as a "more environmentally friendly" near-infrared type of semiconductor material with high absorption coefficient ($\sim 10^5$ cm^{-1}) and narrow bandgap (1.35 eV). Up to now, many reports have focused on the synthesis[26-33] and fluorescence applications[34-36] of InP QDs. The InP QDSSCs, however, were rarely reported. Zaban *et al*. proposed a method to prepare quantum dot solar cells using the InP quantum dots as the sensitizer.[37] The photocurrent and PCE of the solar cells are relatively low, which may be resulted from the corrosive I^-/I^{3-} electrolyte and high electron recombination loss in the QDs/electrolyte interface.[4] Recent studies have reported some approaches to inhibit the charge loss at the interface.[25, 38-42] For examples, the short-circuit current density (J_{sc}), open-circuit voltage (V_{oc}), and PCE are significantly improved by coating with ZnS[43] or ZnS/SiO_2.[25] The performance of II-VI QDSSCs was accordingly improved by the following treatments such as the capping ligand-induced self-assembly (CLIS) and ZnS-covering. These results inspired us toward the preparation of a highly efficient InP QDSSCs.

We noticed that the low photocurrent of QDSSCs may be due to the insufficient loading of QDs and high electron loss at the QDs/electrolyte interface. Therefore, it is important to prepare high-quality QDs sensitized electrodes with enough loading and broad absorption range. Although the CLIS sensitization technique has been well developed and the PCE of the resultant QDSSCs up to 8% has been reported on II-VI,[2, 12, 25] there has been few reports on III-V InP QDs. Moreover, broadening the light-harvesting range through increasing the size of QDs is very limited, but doping can be an effective method. For example, Cu doped InP QDs showed tunable absorption and NIR emission.[44] The Sn dopants were introduced into the bulk InP semiconductor to tune the bandgaps.[45] However, the Sn doped InP (Sn:InP) QDs and its photovoltaic applications have never been reported.

In this work, the Sn:InP QDs were synthesized and immobilized onto mesoporous TiO_2 films using the CLIS sensitization technique, and then covered with ZnS passivation layers *via* the successive ionic layer adsorption and reaction (SILAR) approach. The as-prepared Sn:InP QDs sensitized photoanodes were sintered and assembled into the QDSSCs devices. As a result, the resultant Cd-free green Sn:InP solar cell shows a best PCE of 3.54% under AM1.5G one full sun illumination. The present strategy was shown to have a significant enhancement of the photovoltaic performances of InP QDSSCs.

2. Experimental

Chemicals

The following reagents were used in this study: Indium acetate ($In(Ac)_3$, 99.99%, Aldrich), stannous acetate ($Sn(Ac)_2$, 99.99%, Aldrich), myristic acid (MA, >99%, Sigma), 1-octadecene (ODE, 90%, Aldrich), and tris(trimethylsilyl)phosphine ($P(TMS)_3$, 98%, 10 *wt.*% in hexane, Strem), and 3-mercaptopropionic acid (MPA, 98%, Aladdin).

Characterization

UV-vis absorption spectra were obtained using a Shimadzu UV-1800 spectrophotometer. Transmission electron microscopy (TEM) and high resolution TEM (HR-TEM) were performed on a FEI Titan S/TEM with an accelerating voltage of 200 kV. Scanning electron microscopy (SEM) images were obtained using a FEI Sirion-200 microscope, and the element mapping was carried out through an energy dispersive spectrometer (EDS) equipped on the SEM. Inductively coupled plasma atomic emission spectroscopy (ICP-AES, IRIS Advantage ER/S) was used to identify the composition of the Sn:InP QDs. X-ray diffractions (XRD) were measured on a XPERT-PRO diffractometer system. The photocurrent density-voltage (J-V) curves were recorded by a Keithley 2000 source meter under illumination of an AM 1.5G solar simulator (Newport, Oriel class A, 94023A, equipped with a 150 W tungsten lamp). The incident photon-to-current conversion efficiency (IPCE) spectra were collected by a Keithley 2000 multimeter under the illumination of a 150 W tungsten lamp with a monochromator (DK240). Electrochemical impedance spectroscopy (EIS) measurements were carried out on an impedance analyzer (Zahner, Zennium), and the different bias voltages were carried out from 0 V to -0.6 V applying a 20 mV sinusoidal signal with the frequency between 0.1 Hz and 1.0 MHz

Preparation of Sn:InP QDSSCs

The Sn:InP QDSSCs were obtained by the following procedures in sequence: synthesis of QDs, ligand exchange of QDs, fabrication of Sn:InP-sensitized photoanodes and assembly of solar cells.

Synthesis of QDs: The Sn:InP QDs were synthesized according to the modified method reported by Lucey *et al.*[46] QDs with absorption peaks at 533 nm, 570 nm, 600 nm and 630 nm were denoted as QD533, QD570, QD600 and QD630. Hereafter, QD600 was used as a representative to demonstrate the synthesis process: 0.4 mmol $In(Ac)_3$, 0.04 mmol $Sn(Ac)_2$, 1.2 mmol MA and 5 mL ODE were mixed in a three-neck flask, and the flask was evaluated at 110 ℃ for 2 h. The resulting solution was then heated to 280 ℃ under argon flow. Meanwhile 0.2 mmol $P(TMS)_3$ was mixed with 1 mL ODE in a glove box, and the hexane was removed by pumping. The $P(TMS)_3$-ODE mixture was quickly injected into the reaction flask. The reaction mixture was cooled to 270 ℃ by addition of 2 mL ODE and held for 1 h. Finally, the solution was cooled to ambient temperature. The hexane and methanol/acetone (v/v, 1:4) were used to remove excess ligands and byproducts. The QDs were deposited out by addition of acetone and separated by centrifugation way. The products were washed three times by the hexane/acetone (v/v, 1:3) and dispersed in 10 mL hexane.

The Sn:InP QDs with different dopant concentrations (Sn/In molar ratios) were obtained by tuning the molar ratios of $Sn(Ac)_2$ and $In(Ac)_3$. The Sn:InP (Sn/In=0.1) QDs with different absorption peaks were synthesized through controlling the reaction parameters. Typically, the Sn:InP QDs of QD533 and QD570 were synthesized with MA/In ratio of 3 at 250 ℃ and 260 ℃, respectively. The QD600 and QD630 were synthesized with MA/In ratios of 3.5 and 4 at 270 ℃, respectively.

Ligand exchange of QDs: The ligand exchange was carried out according to the reported method:[47] i) The MPA (17-340 μL) was dissolved in 1 mL methanol and the pH value was adjusted to 10-12 by NaOH aqueous solution; ii) The above basic MPA-methanol mixture was added into 4 mL Sn:InP QDs methylene dichloride solution under stirring for 2h; iii) 10 mL deionized water was injected into the above mixture and stirred for another 5 min; iv) The mixture was centrifuged at 3000 r/min for 1 min to accelerate the separation of the methylene dichloride and aqueous phases; v) The MPA-capped Sn:InP QDs were obtained by precipitation and centrifugation procedure with use of acetone; vi) The QDs were dissolved into 0.2 mL deionized water and adjusted pH value to 12.

The exchange efficiency was obtained according to the method reported by Tamang *et al.*[47] Detailed calculation procedure was shown in the ESI information.

Fabrication of Sn:InP-sensitized photoanodes and assembly of solar cells.: At first, the photoanodes were sensitized by Sn:InP QDs according to the literature method.[48] The loading of QDs on TiO_2 films can be estimated according to the literature[23]. After ZnS-covered and sintered, the Sn:InP QDSSCs were immediately assembled with a sandwich structure: photoanode/polysulfide electrolyte/ Cu_2S counter electrode. The active area of each cell is 0.22 cm^2. Finally, the J-V curves and IPCE curves of the Sn:InP QDSSCs were measured. Six parallel samples were assembled and tested for each QDSSC.

3. Results and Discussion

Optical properties and microstructure characteristics of QDs

To evaluate the photovoltaic performance of different QD size, four Sn:InP QDs (Sn/In=0.1) with different size were successfully synthesized by one-pot nucleation doping approach. The optical properties and microstructure characteristics of Sn:InP QDs were characterized using UV-vis spectroscopy, HR-TEM and XRD. Figure 1(a) shows the absorption spectra of Sn:InP QDs with different QD size. The absorption peak of Sn:InP QDs is gradually red-shifted and broadened as the QD size increases. Correspondingly, the bandgap drops from 2.1 eV to 1.78 eV (Table 1), which indicates a convenient manipulation of the bandgaps by quantum size effect. An exponential function between the QDs size and the absorption peak has already been reported in the literature.[49] The size of our Sn:InP QD600 sample matched with the exponential function very well. We also noticed that the absorption peak red-shifted as the reaction time went on (Figure S1). Therefore, the reaction time was fixed for 1h in this study to rule out the uncertainty induced by reaction time.

The structure of Sn:InP QDs was analyzed by XRD as shown in Figure 1(b). The XRD pattern of the resulting QDs matches well with a zinc-blende structure, and the (111), (220) and (311) diffraction peaks are nearly identical to that of undoped InP QDs. A diffraction peak at 20.9° is originated from the residual indium myristate in InP QDs[46]. In addition, the XRD peaks are broadened due to the nanosize effect of the QDs. Figure 1(c) shows a typical HR-TEM image of Sn:InP QDs. An average size of 3.22 ± 0.52 nm (standard percent deviation of 10.5%) is observed. The shape of Sn:InP QDs is nearly spherical, and the

lattice spacing distance of Sn:InP (3.5 Å) is almost equal to that of InP QDs as shown in Figure 1(d). Figure S2 also illustrates the HR-TEM images of undoped InP QDs and Sn:InP QDs with uniform distribution of size.

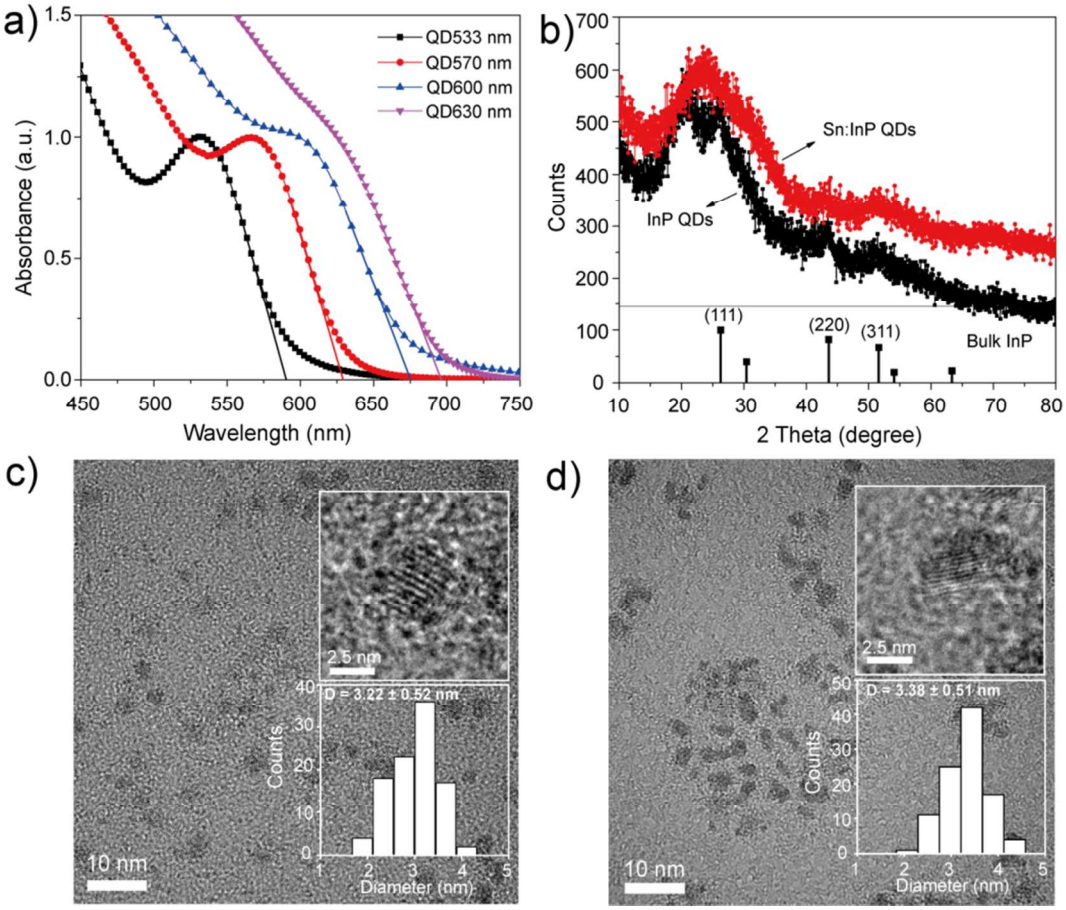

Figure 1. (a) UV-vis spectra of Sn:InP QDs (Sn/In=0.1) with various absorption wavelengths, (b) XRD patterns of InP and Sn:InP QDs. (c) HR-TEM images of Sn:InP QDs and (d) InP QDs. Insets are HR-TEM images and column charts of the size distribution.

Table 1 The bandgaps for different absorption edges (λ_{edge}) of Sn:InP (Sn/In=0.1)

Samples	λ_{edge} / nm	E_g / eV
QD533	590	2.10
QD570	630	1.97
QD600	675	1.84
QD630	695	1.78

Moreover, Sn:InP QDs with different Sn concentrations were obtained by changing the reaction parameters. The Sn/In ratios of Sn:InP QDs were determined by ICP-AES as shown in Table S1. With the variation of Sn/In ratio, a series of Sn:InP QDs with tunable bandgaps were obtained. As shown in Figure S3, the UV-vis spectra of Sn:InP QDs with different Sn/In ratios have a red-shift feature with increasing Sn/In ratios, indicating that the bandgap of InP QDs can be tuned *via* Sn doping. The absorption range of Sn doped InP QDs is wider than that of the undoped ones under the same reaction conditions, which indicates a bandgap modification by Sn doping. To clarify this speculation, we carried out the bandgap calculation of Sn doped InP semiconductor *via* the MS-CASTEP program. Our band structure and density of states (DOS) calculation results indirectly support the UV-vis spectra results, as shown in Figure S4. For Sn doping, the Fermi level upshifts to the bottom of the conduction band of InP, resulting in the formation of n-type doped semiconductors. Meanwhile, the bandgap of Sn:InP is narrower than that of undoped InP. Although the calculated bandgap is underestimated than the result calculated from the absorption edge, the trend of band structure gives the fact that the Sn doping results in n-type InP with a decrease of bandgap.

Optimization of the ligand exchange efficiency

The phase transfer to water-soluble QDs using a ligand-exchange process is an important step for QDSSCs *via* the CLIS sensitization technique. Achieving highly-efficient ligand exchange from hydrophobic phase to hydrophilic phase is critical for improving the loading of QDs on TiO_2 films. Ligand exchange of Sn:InP QDs was accomplished by vigorously stirring a mixed solution of methylene dichloride and basic thiol-containing ligand in methanol. Special zwitterionic organic ligands, such as thioglycolic acid (TGA), MPA and 11-mercaptoundecanoicacid (MUA), have been used as the ligands to prevent the particle aggregation after ligand exchange at basic pH (typically 8-11).[47] The MPA is a common bifunctional linking molecular reagent that has already been chosen to acquire highly-efficient ligand exchange with InP, CdS and CdSe QDs. Moreover MPA facilitates the high wettability and superior penetration capability into hydrophilic TiO_2 films for photoanode sensitizing application. Here, ligand exchange of Sn:InP QDs using MPA was successfully carried out and high exchange efficiency was obtained. In the exchange process, the ligand exchange efficiency was affected by the MPA/QDs molar ratio. It has been reported that high ligand to QDs molar

ratios (such as 10^5:1) are beneficial to the improvement of the exchange efficiency for the InP/ZnS QDs system. In order to obtain the optimal MPA/QDs ratio, the exchange efficiency was tested with various MPA/QDs ratios. When the ligand to QDs ratios gradually increase from 10^4 to 1.7×10^5, the exchange efficiency first increases, then drops as shown in Figure 2. The optimal ratio value of ligand to QDs is 1.7×10^4. At that ratio, the highest exchange efficiency of 74.4% (InP) and 78.0% (Sn:InP) are obtained. Too high or too low MPA/QDs ratios can not improve the exchange efficiency, and even lead to the low loading of QDs on TiO_2 films.

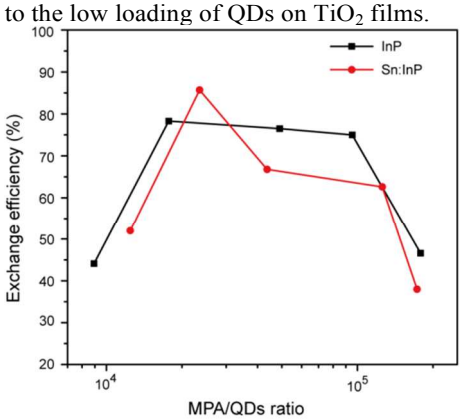

Figure 2. Exchange efficiency with various MPA/QDs ratios

QDs self-assembly on TiO_2 photoanode and loading

High loading of QDs on TiO_2 films is critical to improve the photovoltaic performance of QDSSCs devices.[50] In our work, the CLIS sensitization technique was used for InP QDs system. The Sn:InP QDs with hydrophilic MPA-capped is bound to TiO_2 nanocrystals (~20-40 nm) to form QDs sensitized photoanodes, as shown in Figure 3(a). Dark-brown colored photoanodes were obtained, indicating high loading of QDs. The surface of larger TiO_2 nanoparticles is covered by small size of dots with ~3 nm size, indicating high loading of QDs on the TiO_2 porous channel. The SEM image for the surface of photoanodes is shown in Figure 3(b). It can be observed that the film shows the porous structure with rough surface. The cross-view in Figure 3(c) shows the thickness of the transparent layer TiO_2 is 9 μm. According to the Brunauer-Emmett-Teller (BET) approach, the surface area of our TiO_2 paste was 48.9 m^2/g. The density of the TiO_2 paste is 21.2 g/m^2. The total surface area covered by Sn:InP QDs is about 209 cm^2 and total inner surface area of TiO_2 films is about 1051 cm^2/cm^2. Hence, the maximum loading of Sn:InP QDs are about 20% for Sn:InP QDs. Because of the almost equal absorbance (Figure S5), molar extinction coefficient and diameter with the case of Sn:InP, the loading of InP QDs and Sn:InP QDs are approximately equal. It should be noted that the loading described above was not absolutely equal. To obtain the same loading, same concentrations of the QDs aqueous solution should be used if possible. In order to test the distribution of elements, the surface of photoanodes were characterized by the EDS element mapping. As shown in the inset of Figure 3(b), the In and P elements are uniformly distributed in TiO_2 films. The EDS spectrum of photoanode surface is shown in Figure S6. Because the strong signals of the In L_β peaks (In L_α: 3.28 keV, In L_β: 3.47 keV) tend to overwhelm the weak Sn L_α (3.44 keV) peak, no peaks from Sn are observed. Elemental analysis according to the quantitative analysis software named TEAM, as presented in Table S2, shows the atomic concentrations of In, P and Sn elements are 5.46%, 5.01% and 0.38%, respectively. The Sn/In ratio is consistent with the ICP-AES results (Table S1).

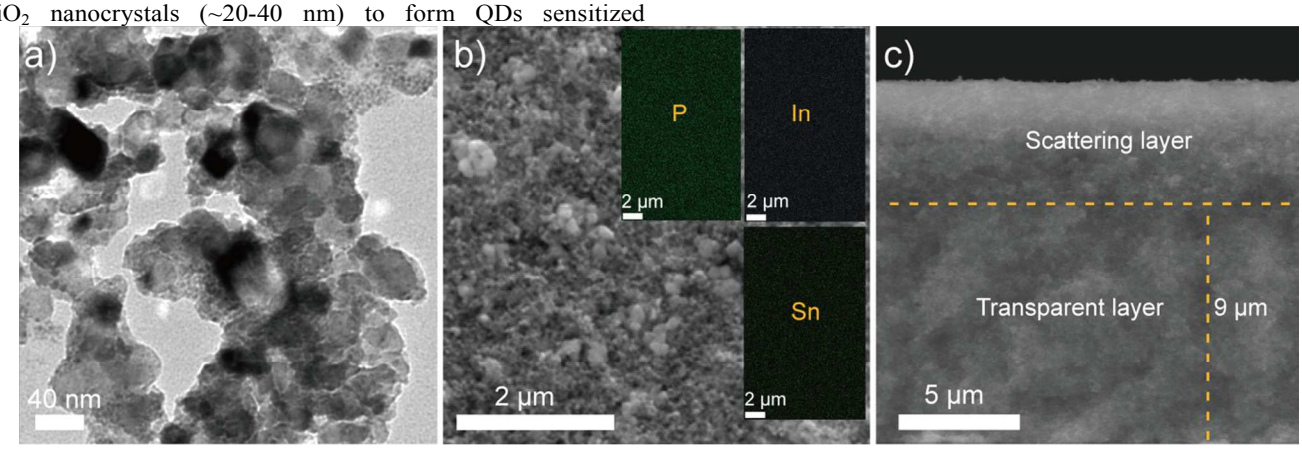

Figure 3. (a) HR-TEM image of TiO_2 nanoparticles loaded with Sn:InP QDs, (b) typical SEM images of top view and (c) cross view of Sn:InP QDs sensitized TiO_2 photoanodes. The insets are the EDS element maping of P, In and Sn.

Photovoltaic Performances

In order to investigate the photovoltaic performances of as-prepared Sn:InP-based QDSSCs, the J-V curves and IPCE curves were recorded. From the J-V curves in Figure 4(a), our best Sn:InP QDSSC device shows a significantly high current density of 10.58 mA/cm^2 and PCE of 3.54%, which is the record efficiency of QDSSCs based III-V QDs. IPCE measurements are used to verify the photocurrent of a solar-cell device. The IPCE value of the best InP and Sn:InP QDSSCs increased from 40% to 55%, as shown in Figure 4(b). The integrated value of the IPCE spectrum of the best Sn:InP QDSSCs involves a short-circuit current density of 10.1 mA/cm^2, which is in good agreement with the measured J_{sc} value of 10.6 mA/cm^2. Moreover, the J-V and IPCE curves of the Sn:InP QDs with different absorption peaks were compared, as shown in Figure 4(c)-(d). Sn:InP QDs with long absorption wavelength have higher short circuit current density than the QDs with short absorption wavelength. However, the QD630 shows lower current density than that of QD600, which could be caused by the broad size distribution of QD630. Nevertheless, the distribution of large Sn:InP QDs needs to be further controlled in our future work. The IPCE curves of Sn:InP with various absorption peaks are consistent with the J-V curves.

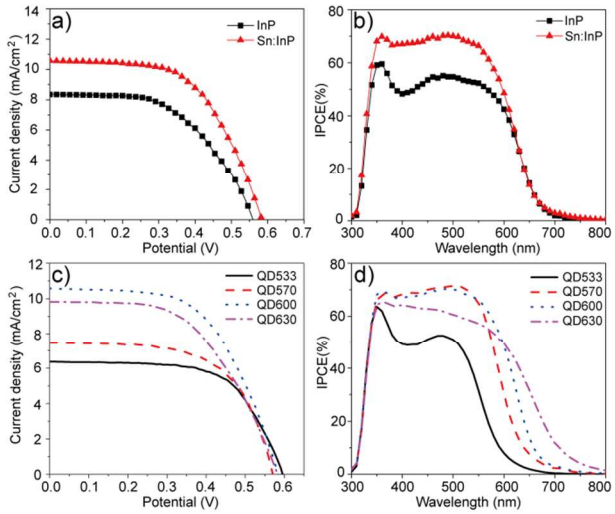

Figure 4. (a) J-V characteristic curves, (b) IPCE curves of InP, Sn:InP QDSSCs, (c) J-V curves and (d) IPCE curves of Sn:InP QDSSCs with various absorption wavelengths.

As shown in Table 2, the photocurrent of our InP QDSSCs is higher than the result reported previously.[37] Some improvements were adopted in our InP QDSSCs devices. Firstly, the ZnS-covering treatment was carried out by SILAR approach in our experiments. Figure 5 shows that both J_{sc} and V_{oc} are significantly improved in Sn:InP QDSSCs in the presence of ZnS passivation layer, indicating an effective inhibition of electron recombination loss on the QDs/electrolyte interface.[51] Secondly, the counter electrodes of Pt and polyiodide electrolyte were replaced by Cu_2S counter electrode and polysulfide electrolyte, respectively.

Our results demonstrate that stable and high efficiency cell devices can be obtained. In addition, the scattering TiO_2 layer was used to enhance the harvest of sunlight. Indeed, the previous work[37] is the first demonstration of a QD sensitized cell using polyiodide as electrolyte, which is known to be improper for QD-based devices. Nowadays, it is well known that the iodide/triiodide electrolyte is strongly photocorrosive for QDs, leading to rapid decreases of photocurrent.[5] Comparisons of photocurrent in CdS QDSSCs with iodide/triiodide and polysulfide electrolytes have already been reported by Tachibana *et al.*[52] The iodide/triiodide electrolyte generated lower values of photocurrent and had very short durability (100 s). Compared to the iodide/triiodide electrolyte, the polysulfide electrolyte [redox potential E_{red}: -0.45 V *vs* normal hydrogen electrode (NHE)] generated more stable photocurrents and longer lifetime.[14]

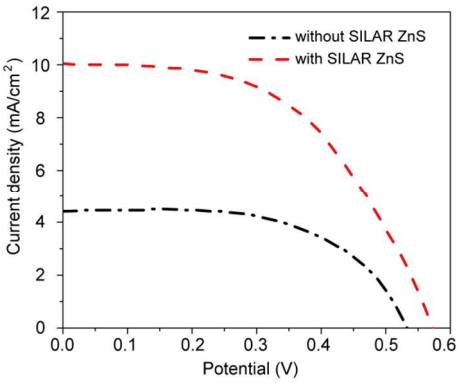

Figure 5. I-V curves of Sn:InP QDSSCs device with SILAR ZnS and without SILAR ZnS

Moreover, a lower fill factor (FF <50%) was obtained when using Pt counter electrode at QDSSCs with polysulfide electrolytes. Cu_2S counter showed highly electrocatalytical activity and high FF for polysulfide electrolyte than Pt counter electrode.[53] Hence, we assembled the Sn:InP QDSSCs employing ZnS-passivated photoanode, polysulfide electrolyte and Cu_2S counter electrode, which exhibited significant improvements comparing with the earlier work.[37] Furthermore, high loading of Sn:InP QDs and broad absorption range enhanced the short-circuit current density.

In addition, the dependences of photovoltaic performances on the TiO_2 film thickness and Sn dopant concentration were also investigated systematically as shown in Figure S7. The optimal thickness of 9 μm and Sn/In ratio of 0.1 were obtained. The effects of over-high Sn/In ratios probably cause many defects with P dangling bonds. The best Sn/In ratio is 0.1 in our experiments, providing the highest PCE efficiency.

The stability property of the Sn:InP QDSSCs was studied under continuous illumination as shown in Figure S8. The photocurrent densities of cell devices were recorded once per minute under continuous illumination. The photocurrent remains steady at 10 mA/cm^2 during 12 min and then quickly fall to 8.6 mA/cm^2. The PCE of the Sn:InP QDSSCs under continuous illumination shows the same trend and the PCE value remains steady at 3.3% during 12 min, indicating similar good stability to the CdSe QDSSCs with the same counter electrodes[54]. Although the lifetime of the Sn:InP QDSSCs device is not long enough, further investigation on the improvement of stability will give the new prospect for III-V InP QDSSCs.

Table 2. Photovoltaic performance of our best InP-based cells and III-V QDSSCs from literature under AM1.5 illumination

Cells	Size (nm)	J_{sc} (mA/cm^2) [a]	V_{oc} (V) [a]	FF (%) [a]	PCE (%) [a]	IPCE (%) [b]
InP	3.2	8.36 (8.20 ± 0.44)	0.56 (0.56 ± 0.01)	54.8 (56.0 ± 3.2)	2.57 (2.56 ± 0.03)	40
Sn:InP (QD600)	3.22	10.58 (10.33 ± 0.21)	0.59 (0.58 ± 0.01)	56.7 (56.6 ± 1.3)	3.54 (3.38 ± 0.08)	55
InP[37]	6.5	0.24	0.56	68	<0.1	<2

[a]The best values are given, followed by the averages and standard deviations from 6 devices. [b]IPCE tested from the best cells.

Impedance spectroscopy

In order to investigate the electron loss of Sn:InP QDSSCs, we measured the EIS in dark conditions at different applied bias voltages (V_{appl}) from 0 V to -0.6 V with frequencies between 0.1 Hz and 1 MHz, and the results are shown in Figure 6. The dependences of recombination resistance (R_{rec}), shunted chemical capacitance (C_μ) and dark current on the V_{appl} are illustrated in Figure 6(a)-(c). Figure 6(d) gives the nyquist curves of the InP and Sn:InP cells at a forward bias near the V_{oc} of the cells, and the extracted parameters are collected in Table 3. R_{rec} and C_μ are related to the charge recombination at the interface of QDs and TiO_2 and electrolyte. The value of R_{rec} of

Sn:InP QDSSCs is about 1.4 times that of undoped InP, and eight times higher than that recorded for CdSe at the same bias voltage. The C_μ value of InP-base device is lower than that of CdSe. As a result, the recombination electron lifetime (τ_n=R_{rec}×C_μ) value of 201.5 ms of the Sn:InP QDSSCs is 1.4 times higher than that of undoped InP. The lifetime is slightly higher than the recorded data for CdSe (185.5 ms) CdSe,[55] indicating the blockage of charge recombination and the recombination rate of electrons of the Sn:InP. The high recombination resistance and long electron lifetime provide an enhancement of the photovoltaic performances. Approximate equal recombination resistances was observed from the nyquist curves of Sn:InP QDSSCs with different absorption wavelengths (Figure S9), indicated the weak correlation between the recombination resistances and size of QDs. However, the ohmic serial resistance (R_s) of 18.5 Ω/cm^2 of Sn:InP QDSSCs is several times higher than that of CdSe QDSSC, indicating high electron transfer loss from Sn:InP QDs to TiO_2. This high R_s value is mainly caused by high transfer resistances of FTO/TiO_2 and QDs/TiO_2 interface, and further investigation to improve the electron transfer will be conducted concerning in our experiments.

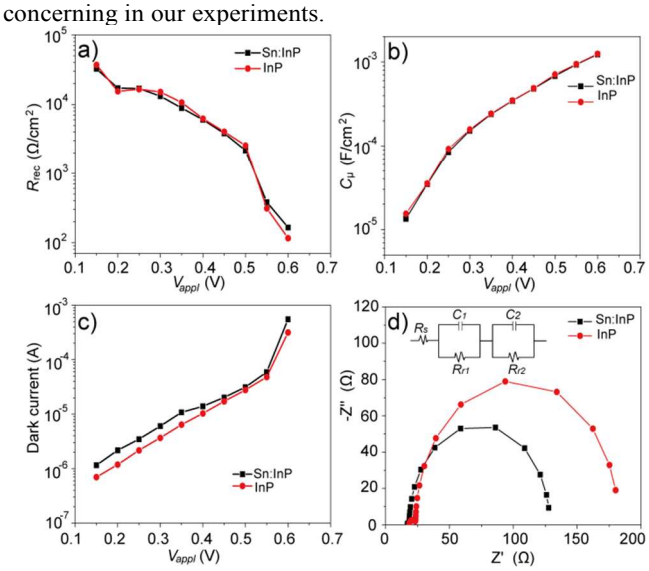

Figure 6. Electrochemical impedance spectroscopy of Sn:InP and InP QDSSCs. (a) recombination resistance, R_{rec}, (b) chemical capacitance, C_μ, (c) dark currents, and (d) Nyquist curves of these device at -0.6 V bias. The inset shows the corresponding equivalent circuit model for fitting EIS.

Table 3. EIS data under bias voltage of -0.6 V for the best device of InP and Sn:InP QDSSC

Cells	R_s Ω/cm^2	R_{ce} Ω/cm^2	C_{ce} μF/cm^2	R_{rec} Ω/cm^2	C_μ mF/cm^2	τ ms
InP	17.0	1.5	79.2	115.9	1.25	144.5
Sn:InP	18.5	5.0	49.2	165.2	1.22	201.5
CdSe[56]	4.82	0.22	43.7	20.52	9.04	185.5

4. Conclusions

In conclusion, high quality InP based QDs with tunable absorption range were synthesized and characterized. For the first time, the CLIS sensitization technique is adopted for the III-V QD system in the construction of QDSSCs. With the optimization of ligand exchange process and the content of Sn dopant in the host InP QDs, a moderate PCE of 3.5% has been obtained. The high ligand-exchange efficiency, large loading of QDs and ZnS passivation layer *via* the CLIS sensitization technique provide high quality photoanodes. Combining the suitable polysulfide electrolyte and Cu_2S counter electrodes, high efficient InP QDs based QDSSCs were obtained. The presence of Sn dopant obviously increased the photocurrent density and efficiency of InP QDSSCs because of the effective regulation of the absorption edge of InP QDs. This work provides an important step toward developing highly-efficient quantum dot photovoltaic devices. Continuous improvement for doped InP QDs solar cells should produce higher PCE in the near future.

Author Information

Corresponding Author: Xinchun Lai. E-mail: laixinchun@caep.cn.

Acknowledgements

The authors acknowledge the assistance of Chun-Li Jiang, Qin-Yin Xu and Rong-Guang Zen in SEM and HR-TEM sample characterization and data interpretation. The authors also thank Dr. Xiao-Fang Wang and Rui-Zhu Yang for helpful discussion. This research was funded by the Special Research Found for development of key disciplinary areas program (ZDXKFZ201217).

Notes

Electronic Supplementary Information (ESI) available: Detailed calculation procedures of ligand exchange yield. Temporal evolution of absorption spectra of Sn:InP QDs. The HR-TEM images of the oil-soluble Sn:InP QDs. Absorption spectra of InP QDs with different Sn dopant concentration. The Band-DOS curves of calculated. EDS spectra of QDs sensitized TiO_2 films. The stability properties of the Sn:InP QDSSCs. Nyquist curves of Sn:InP QDSSCs with different absorption wavelength. This material is available free of charge *via* the Internet at http://www.rsc.org.

References

1. M. C. Hanna and A. J. Nozik, *J. Appl. Phys.*, 2006, **100**.
2. W. J. Li and X. H. Zhong, *J. Phys. Chem. Lett.*, 2015, **6**, 796-806.
3. W. J. Li and X. H. Zhong, *Acta Phys. Sin-Ch. Ed.*, 2015, **64**.
4. I. Mora-Sero, S. Gimenez, F. Fabregat-Santiago, R. Gomez, Q. Shen, T. Toyoda and J. Bisquert, *Acc. Chem. Res.*, 2009, **42**, 1848-1857.
5. Z. Yang, C. Y. Chen, P. Roy and H. T. Chang, *Chem. Commun.*, 2011, **47**, 9561-9571.
6. M. Kouhnavard, S. Ikeda, N. A. Ludin, N. B. Ahmad Khairudin, B. V. Ghaffari, M. A. Mat-Teridi, M. A. Ibrahim, S. Sepeai and K. Sopian, *Renew. Sust. Energ. Rev.*, 2014, **37**, 397-407.
7. T. Li, X. Zou and H. Zhou, *Int. J. Photoenergy*, 2014, **2014**, 1-6.
8. S. S. Mali, S. K. Desai, S. S. Kalagi, C. A. Betty, P. N. Bhosale, R. S. Devan, Y. R. Ma and P. S. Patil, *Dalton Trans.*, 2012, **41**, 6130-6136.
9. R. Ahmed, L. Zhao, A. J. Mozer, G. Will, J. Bell and H. X. Wang, *J. Phys. Chem. C*, 2015, **119**, 2297-2307.
10. S.-Q. Fan, D. Kim, J.-J. Kim, D. W. Jung, S. O. Kang and J. Ko, *Electrochem. Commun.*, 2009, **11**, 1337-1339.
11. B. Gao, C. Shen, S. L. Yuan, B. Zhang, M. Y. Zhang, Y. X. Yang and G. R. Chen, *J. Alloys Compd.*, 2014, **612**, 323-329.
12. S. Jiao, Q. Shen, I. Mora-Sero, J. Wang, Z. X. Pan, K. Zhao, Y. Kuga, X. H. Zhong and J. Bisquert, *ACS nano*, 2015, **9**, 908-915.
13. A. P. Kumar, B. T. Huy, B. P. Kumar, J. H. Kim, V. D. Dao, H. S. Choi and Y. I. Lee, *J. Mater. Chem. C*, 2015, **3**, 1957-1964.
14. Y. L. Lee, B. M. Huang and H. T. Chien, *Chem. Mater.*, 2008, **20**, 6903-6905.

15. J. J. Tian, R. Gao, Q. F. Zhang, S. G. Zhang, Y. W. Li, J. L. Lan, X. H. Qu and G. Z. Cao, *J. Phys. Chem. C*, 2012, **116**, 18655-18662.
16. H. J. Yun, T. Paik, M. E. Edley, J. B. Baxter and C. B. Murray, *ACS Appl. Mater. Interfaces*, 2014, **6**, 3721-3728.
17. J. Y. Chang, J. M. Lin, L. F. Su and C. F. Chang, *ACS Appl. Mater. Interfaces*, 2013, **5**, 8740-8752.
18. D. H. Jara, S. J. Yoon, K. G. Stamplecoskie and P. V. Kamat, *Chem. Mater.*, 2014, **26**, 7221-7228.
19. T.-L. Li, Y.-L. Lee and H. Teng, *Energy Environ. Sci.*, 2012, **5**, 5315-5324.
20. Z. Peng, Y. Liu, W. Shu, K. Chen and W. Chen, *Chem. Phys. Lett.*, 2013, **586**, 85-90.
21. P. K. Santra, P. V. Nair, K. George Thomas and P. V. Kamat, *J. Phys. Chem. Lett.*, 2013, **4**, 722-729.
22. W. J. Li, Z. X. Pan and X. H. Zhong, *J. Mater. Chem. A*, 2015, **3**, 1649-1655.
23. H. Zhang, K. Cheng, Y. M. Hou, Z. Fang, Z. X. Pan, W. J. Wu, J. L. Hua and X. H. Zhong, *Chem Commun (Camb)*, 2012, **48**, 11235-11237.
24. Z. Pan, I. Mora-Sero, Q. Shen, H. Zhang, Y. Li, K. Zhao, J. Wang, X. Zhong and J. Bisquert, *J. Am. Chem. Soc.*, 2014, **136**, 9203-9210.
25. K. Zhao, Z. Pan, I. Mora-Seró, E. Cánovas, H. Wang, Y. Song, X. Gong, J. Wang, M. Bonn, J. Bisquert and X. Zhong, *J. Am. Chem. Soc.*, 2015, **137**, 5602-5609.
26. S. Joung, S. Yoon, C. S. Han, Y. Kim and S. Jeong, *Nanoscale Res. Lett.*, 2012, **7**, 93.
27. K. Lim, H. S. Jang and K. Woo, *Nanotechnology*, 2012, **23**, 485609.
28. H. Virieux, M. Le Troedec, A. Cros-Gagneux, W. S. Ojo, F. Delpech, C. Nayral, H. Martinez and B. Chaudret, *J. Am. Chem. Soc.*, 2012, **134**, 19701-19708.
29. B. R. Liu, J. G. Winiarz, J. S. Moon, S. Y. Lo, Y. W. Huang, R. S. Aronstam and H. J. Lee, *Colloids Surf. B Biointerfaces*, 2013, **111**, 162-170.
30. W. E. Mahmoud, Y. C. Chang, A. A. Al-Ghamdi, F. Al-Marzouki and L. M. Bronstein, *Superlattices Microstruct.*, 2013, **56**, 86-91.
31. P. Mushonga, M. O. Onani, A. M. Madiehe and M. Meyer, *Mater. Lett.*, 2013, **95**, 37-39.
32. N. Mordvinova, P. Emelin, A. Vinokurov, S. Dorofeev, A. Abakumov and T. Kuznetsova, *Beilstein J. Nanotech.*, 2014, **5**, 1220-1225.
33. N. Mordvinova, A. Vinokurov, S. Dorofeev, T. Kuznetsova and K. Znamenkov, *J. Alloys Compd.*, 2014, **582**, 43-49.
34. L. M. Lacroix, F. Delpech, C. Nayral, S. Lachaize and B. Chaudret, *Interface focus*, 2013, **3**, 20120103.
35. S. J. Soenen, B. B. Manshian, T. Aubert, U. Himmelreich, J. Demeester, S. C. De Smedt, Z. Hens and K. Braeckmans, *Chem. Res. Toxicol.*, 2014, **27**, 1050-1059.
36. X. Zhang, H. Chibli, D. Kong and J. Nadeau, *Nanotechnology*, 2012, **23**, 275103.
37. A. Zaban, O. I. Micic, B. A. Gregg and A. J. Nozik, *Langmuir*, 1998, **14**, 3153-3156.
38. B. Ehrler, K. P. Musselman, M. L. Bohm, F. S. Morgenstern, Y. Vaynzof, B. J. Walker, J. L. Macmanus-Driscoll and N. C. Greenham, *ACS nano*, 2013, **7**, 4210-4220.
39. A. Badawi, *Chinese Phys B*, 2015, **24**.
40. N. Balis, V. Dracopoulos, K. Bourikas and P. Lianos, *Electrochim. Acta*, 2013, **91**, 246-252.
41. H. Seo, Y. Wang, G. Uchida, K. Kamataki, N. Itagaki, K. Koga and M. Shiratani, *Electrochim. Acta*, 2013, **87**, 213-217.
42. X. J. Shi, Y. Wang, D. P. Wu, Y. J. Qin, X. C. Ai, D. S. Xu and J. P. Zhang, *Rsc Adv*, 2015, **5**, 32110-32117.
43. Q. Shen, J. Kobayashi, L. J. Diguna and T. Toyoda, *J. Appl. Phys.*, 2008, **103**.
44. R. Xie and X. Peng, *J. Am. Chem. Soc.*, 2009, **131**, 10645-10651.
45. D. Cai and J. Kang, *J. Appl. Phys.*, 2007, **102**, 103518.
46. D. W. Lucey, D. J. MacRae, M. Furis, Y. Sahoo, A. N. Cartwright and P. N. Prasad, *Chem. Mater.*, 2005, **17**, 3754-3762.
47. S. Tamang, G. Beaune, I. Texier and P. Reiss, *ACS nano*, 2011, **5**, 9392-9402.
48. Z. Du, H. Zhang, H. Bao and X. Zhong, *J. Mater. Chem. A*, 2014, **2**, 13033.
49. R. Xie, Z. Li and X. Peng, *J. Am. Chem. Soc.*, 2009, **131**, 15457-15466.
50. N. Guijarro, T. Lana-Villarreal, I. Mora-Sero, J. Bisquert and R. Gomez, *J. Phys. Chem. C*, 2009, **113**, 4208-4214.
51. N. Guijarro, J. M. Campina, Q. Shen, T. Toyoda, T. Lana-Villarreal and R. Gomez, *PCCP*, 2011, **13**, 12024-12032.
52. Y. Tachibana, H. Y. Akiyama, Y. Ohtsuka, T. Torimoto and S. Kuwabata, *Chem. Lett.*, 2007, **36**, 88-89.
53. K. Zhao, H. Yu, H. Zhang and X. Zhong, *J. Phys. Chem. C*, 2014, **118**, 5683-5690.
54. H. Zhang, H. L. Bao and X. H. Zhong, *J. Mater. Chem. A*, 2015, **3**, 6557-6564.
55. J. Wang, I. Mora-Sero, Z. Pan, K. Zhao, H. Zhang, Y. Feng, G. Yang, X. Zhong and J. Bisquert, *J. Am. Chem. Soc.*, 2013, **135**, 15913-15922.
56. Z. Pan, H. Zhang, K. Cheng, Y. Hou, J. Hua and X. Zhong, *ACS nano*, 2012, **6**, 3982-3991.

Graphical Abstract

The InP and Sn doped InP (Sn:InP) based quantum dot sensitized solar cells with a moderate efficiency were successfully fabricated.